International Journal of Mining Science and Technology xxx (xxxx) xxx

Contents lists available at ScienceDirect

International Journal of Mining Science and Technology

journal homepage: www.elsevier.com/locate/ijmst

Review Article

Gouge stability controlled by temperature elevation and obsidian addition in basaltic faults and implications for moonquakes

Shutian Cao [a,b], Fengshou Zhang [a,b,*], Mengke An [a,b,*], Derek Elsworth [c,d], Manchao He [e], Hai Liu [f], Luanxiao Zhao [g]

[a] Department of Geotechnical Engineering, College of Civil Engineering, Tongji University, Shanghai 200092, China
[b] Key Laboratory of Geotechnical & Underground Engineering of Ministry of Education, Tongji University, Shanghai 200092, China
[c] Department of Energy and Mineral Engineering, EMS Energy Institute and G3 Center, The Pennsylvania State University, University Park, PA 16802, USA
[d] Department of Geosciences, The Pennsylvania State University, University Park, PA 16802, USA
[e] State Key Laboratory for Geomechanics and Deep Underground Engineering, China University of Mining and Technology-Beijing, Beijing 100083, China
[f] School of Civil Engineering, Guangzhou University, Guangzhou 510006, China
[g] School of Ocean and Earth Sciences, Tongji University, Shanghai 200092, China

ARTICLE INFO

Article history:
Received 12 November 2023
Received in revised form 6 April 2024
Accepted 23 April 2024
Available online xxxx

Keywords:
Fault stability
Basaltic fault
Temperature elevation
Obsidian content
Shallow moonquakes

ABSTRACT

Basalt is a major component of the earth and moon crust. Mineral composition and temperature influence frictional instability and thus the potential for seismicity on basaltic faults. We performed velocity-stepping shear experiments on basalt gouges at a confining pressure of 100 MPa, temperatures in the range of 100–400 °C and with varied obsidian mass fractions of 0–100% under wet/dry conditions to investigate the frictional strength and stability of basaltic faults. We observe a transition from velocity-neutral to velocity-weakening behaviors with increasing obsidian content. The frictional stability response of the mixed obsidian/basalt gouges is characterized by a transition from velocity-strengthening to velocity-weakening at 200 °C and another transition to velocity-strengthening at temperatures >300 °C. Conversely, frictional strengths of the obsidian-bearing gouges are insensitive to temperature and wet/dry conditions. These results suggest that obsidian content dominates the potential seismic response of basaltic faults with the effect of temperature controlling the range of seismogenic depths. Thus, shallow moonquakes tend to occur in the lower lunar crust due to the corresponding anticipated higher glass content and a projected temperature range conducive to velocity-weakening behavior. These observations contribute to a better understanding of the nucleation mechanism of shallow seismicity in basaltic faults.

Contents

* Corresponding authors.
E-mail addresses: fengshou.zhang@tongji.edu.cn (F. Zhang), 2015mengkean@tongji.edu.cn (M. An).

https://doi.org/10.1016/j.ijmst.2024.04.012
2095-2686/

Please cite this article as: S. Cao, F. Zhang, M. An et al., Gouge stability controlled by temperature elevation and obsidian addition in basaltic faults and implications for moonquakes, International Journal of Mining Science and Technology, https://doi.org/10.1016/j.ijmst.2024.04.012

1. Introduction

Basalt is the main component of both the terrestrial oceanic crust and the lunar mare crust and also an important component of the terrestrial continental crust [1,2]. Plagioclase and pyroxene are the main constituents of basalt. In addition, basaltic glasses are a quenched product of basaltic melts and a common component of the oceanic crust and host to numerous large earthquakes [3]. As seismic response is controlled by the frictional evolution of faults [4], characterization of the frictional properties of basalt faults is important in defining earthquake characteristics and hazards. Recorded seismic events designated as "moonquakes" result from meteorite impacts and the triggering of shallow and deep reactivation on faults [5]. Among these, the shallow moonquakes, observed in the lunar crust and exhibiting larger magnitudes, are substantially similar to intraplate earthquakes on Earth [6], and are the most deserving of attention. In addition, high in situ temperatures in the lower crust may play a key role in defining the frictional response [7]. Thus, further characterization of the effects of mineral components and temperatures on the frictional strength and stability of basaltic faults is important.

The presence of interstitial glass potentially contributes significant complexity in understanding the response of basaltic faults [8]. Lunar glass is the main component of lunar soil [9,10], composed of endogenous volcanic glass (i.e., obsidian) from the quenching of lunar magmas and exogenous impact glass from quenching during impact events [11]. Glass is also a significant component of subduction thrust zones, together with clays as pore-filling precipitates, serving as weaker and more easily fractured regions [12]. Additionally, a millimeter-scale trail of quenched glass (i.e., pseudotachylyte) can rapidly solidify following frictional surface melting from high velocity slips during earthquakes [13]. These observations infer that glass potentially exhibits a crucial control on the frictional properties of lunar rocks, subduction zones, and other basaltic faults containing glass. Prior studies mainly focus on the frictional properties of pure volcanic glasses. At temperatures $\leq$300 °C, dry glass gouges, including soda-lime glass [14], rhyolitic glass [15] and silica glass [16] exhibit frictional properties similar to granite and quartz gouges. Glass exhibits a mechanical transition from brittle to plastic at temperatures >400 °C [17]. Moreover, the presence of water has been proven to significantly lower the transition temperature [15]. In sum, these collective investigations on the frictional properties of glass-filled basaltic faults remain insufficient and recent investigations only highlight the importance of glass in promoting earthquake rupture [8].

The high temperatures present at multi-kilometer depths govern fault slip stability in the Earth's crust [18]. Previous studies conducted under hydrothermal conditions on common mafic rock gouges, including gabbro [19], plagioclase [20,21], basalt [22,23], and pyroxene [20] show a translation in fault frictional stability from velocity-strengthening/neutral to velocity-weakening then returning to velocity-neutral/strengthening at elevated temperatures. The velocity-weakening stage spans the temperature range of 250–600 °C. As a counterpoint, the temperature of the lunar crust ranges from −180 to 600 °C with increasing depth [24], so this stability transition with temperature can be a vital factor in controlling the propensity for faulting and seismicity. However, the underlying mechanism for the deformation of fault gouges transitions at different temperatures (especially high temperatures) and for different mineral compositions. Plastic flow at asperity contacts [14] and pressure solution [25,26] are both widely accepted interpretations affecting structural change [21,27] and impacting macroscale response. Thus, detailed characterization of transition temperatures on fault frictional stability and reasonable interpretations of governing mechanisms are needed.

To this end, we inspect the impacts of temperatures and mineral composition (especially the effect of obsidian) on the frictional strength and stability of basalt faults at conditions relevant to the lunar crust at 20 km (equivalent to terrestrial crust at ~6 km). It is worth noting that we selected obsidian as the lunar glass in this work to simulate the lunar crust which contains only endogenous volcanic glass and hosts shallow moonquakes. Prior works on lunar rock simulants have encompassed various simulation criteria, such as mineral composition, particle size distribution, and element distribution [28,29]. In this work, we specifically concentrate on the mineral composition. Velocity-stepping experiments are conducted at obsidian mass fractions of 0–100%, with the temperatures in the range of 100–400 °C under wet/dry conditions. Then, we further analyze these observations and compare them to prior results to better understand implications for both shallow moonquakes and seismicity within Earth's crust.

2. Materials and methods

2.1. Sample materials

We collected natural basalt and obsidian, removed soil-like impurities then powdered and sieved the samples to particle sizes less than 75 μm as the representative of fault gouges. The mineral composition of the basalt by mass fraction is ~36% anorthite, ~42% diopside, ~19% forsterite, ~1% lawsonite and ~2% pyrite, according to X-ray diffraction (XRD) results (Fig. 1). In addition, the obsidian mineral exhibits a completely amorphous state. It is worth noting that the selected basalt has similar composition by % fractions to lunar mare basalt (e.g., CE-5 lunar soil samples contain 30.1% plagioclase, 30.9% augite, 11.1% pigeonite, 4.5% ilmenite, 4.1% fayalite, 1.6% forsterite, and 16.6% glass by mass fraction) [9,10].

2.2. Experimental procedures

Shear experiments were performed on a triaxial shear apparatus with argon-gas confined (Fig. 1c) at the Institute of Geology, China Earthquake Administration, Beijing, China, with details about this apparatus by He et al. [19]. This apparatus can apply temperatures to 600 °C, confining pressures to 420 MPa and pore fluid pressures to 200 MPa. In the shear experiments, a 1 mm-thick gouge layer was placed between two cylindrical gabbro driving blocks, each with a diameter of 20 mm and a height of 40 mm, that were cut at a 35° angle to the loading axis. The saw-cut surfaces of the two blocks were polished by 200-mesh silicon carbide to avoid boundary slippage. An injection hole was drilled through the upper block for deionized water to access the sample as the pressurized pore fluid, with a brass filter capping the injection hole to prevent gouge extrusion. The assembled sample, sandwiched

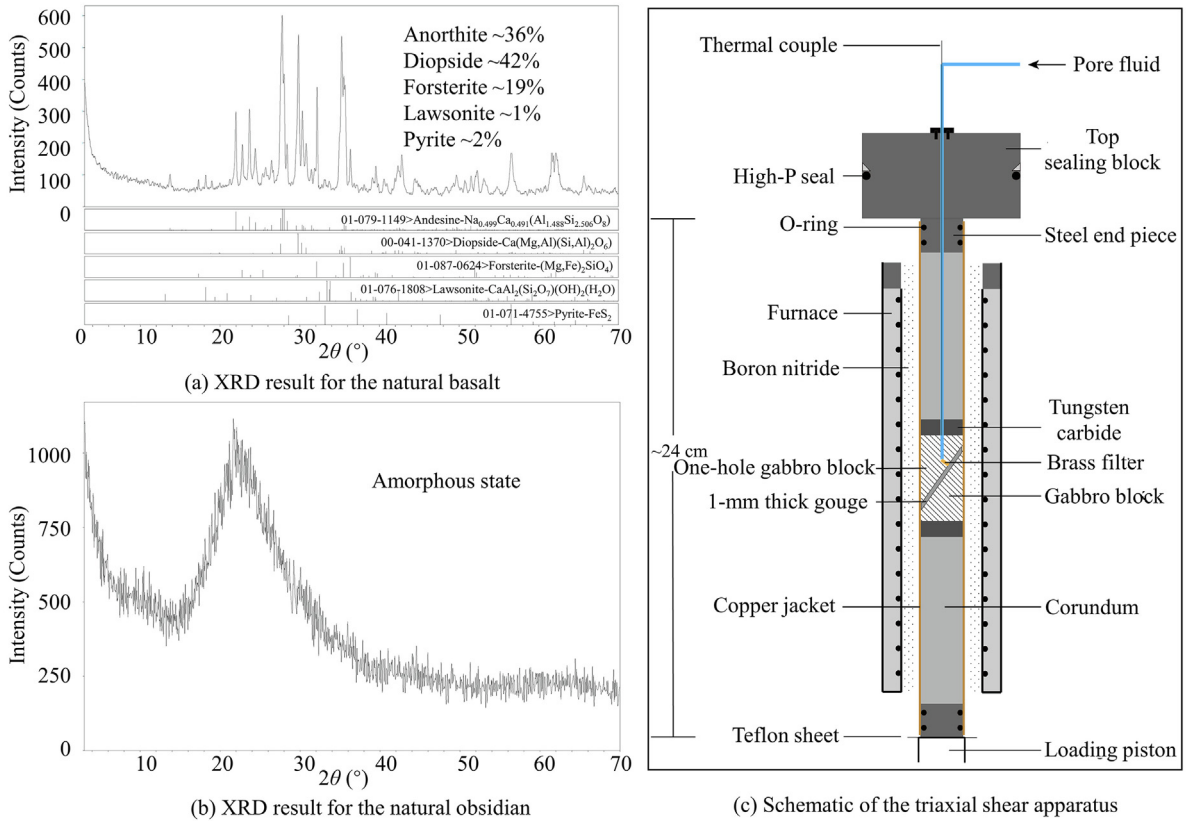

Fig. 1. Basic information for samples and apparatus.

Table 1
Matrix of experimental conditions and main data.

Experimental groups	Test ID	Basalt mass fraction (%)	Obsidian mass fraction (%)	σ_c (MPa)	P_f (MPa)	T (°C)	l_{final} (mm)	Fault response
Group 1: Variable mineral content	LC1	100	0	100	0	200	3.83	vs/vn
	LC2	80	20	100	0	200	3.51	vn
	LC3	50	50	100	0	200	3.58	vw
	LC4	0	100	100	0	200	3.72	vw
Group 2: Variable temperature	LC5	80	20	100	0	100	3.59	vs
	LC6	80	20	100	0	250	3.61	vn/vw
	LC7	80	20	100	0	300	3.72	vn
	LC8	80	20	100	0	400	3.58	vs
Group 3: Variable humidity (wet)	LC9	0	100	110	10	200	3.72	vw/ss

Note: σ_c stands for the confining pressure; P_f the pore fluid pressure; T the temperature; l_{final} the final shear displacement; vs the velocity-strengthening; vn the velocity-neutral; vw the velocity-weakening; and ss the stick–slip.

between tungsten carbide and high-hardness corundum forcing blocks, was encased in a 0.35 mm thick annealed copper jacket. Double O-rings were used to seal the top and bottom of the sample, preventing any gas leakage. (Fig. 1c). The assembled sample was subjected to argon gas confining pressure and heated by an internal furnace while temperature was monitored with a thermocouple. The gap between the furnace and the sample was filled with boron nitride to prevent gas convection. Axial displacement was driven through an electro-hydraulic servo-control system. Additionally, wet gouges were saturated for 2 h to ensure complete saturation after applying pore fluid pressure, while dry gouges were heated at 250 °C for 2 h to ensure fully-dry conditions before shearing.

We designed two main groups of shear experiments on powered dry gouges with an extra experiment under hydrothermal conditions—with details shown in Table 1. Experiments in Group 1 on mixed basalt/obsidian gouges were conducted to investigate the effect of obsidian content on the friction behavior of basalt faults (Test IDs: LC1, LC2, LC3, and LC4). In Group 2, we explore the effects of temperature variation on gouge frictional strength and stability (Test IDs: LC5, LC2, LC6, LC7, and LC8). All experiments conducted on dry gouges were performed at a constant confining stress of 100 MPa to approximate the lithostatic (rock density of ~3000 kg/m^3) at 20 km depth within the lunar crust. Experimental temperatures were defined from previous lunar temperature profile models [24]. In Group 3, we added an additional test (Test ID: LC9) on obsidian gouge under hydrothermal conditions to investigate the effect of humidity under a constant effective confining pressure, as in previous tests. The gouges were initially sheared at an axial displacement velocity of 1 μm/s till a

steady state friction was reached, then stepped between rates of 1.0, 0.2, and 0.04 μm/s (equivalent to the shear rates in the shear direction: 1.22, 0.244, and 0.0488 μm/s).

2.3. Data analysis

The experimental data, including the confining pressure, piston load, pore fluid pressure, temperature, and axial displacement were recorded at a sampling frequency of 1 Hz. Following the method described by He et al. [19], the raw experimental data were then corrected to eliminate the effect of decreasing contact area with increasing shear offset of the inclined fracture and the shear resistance of the copper jacket. The friction coefficient μ was calculated from

$$\mu = \frac{\tau}{\sigma_n} \tag{1}$$

where τ and σ_n denote the shear and normal stresses been corrected, respectively. The velocity dependence parameter $(a-b)$ was then derived by using rate-state-friction (RSF) theory [30,31]. In the RSF theory framework, the friction coefficient μ is indicated as

$$\mu = \mu_0 + a\ln\left(\frac{V}{V_0}\right) + b\ln\left(\frac{V_0\theta}{d_c}\right) \tag{2}$$

$$\frac{d\theta}{dt} = 1 - \frac{V\theta}{d_c} \tag{3}$$

where μ and μ_0 are the friction coefficient at the instantaneous shear velocity V and the reference shear velocity V_0, respectively; a and b the dimensionless constants representing the direct and evolutionary effects in a velocity step, respectively; the state variable θ denotes frictional contact age; and d_c the critical slip distance needed to achieve a new steady state. At steady state friction, Eq. (3) can be reduced to $V\theta = d_c$. Therefore, the frictional stability parameter $(a-b)$ can be calculated as

$$a - b = \frac{\Delta\mu_{ss}}{\Delta\ln V} \tag{4}$$

where μ_{ss} denotes the difference in the friction coefficient between two continuous steady states. Faults with positive $(a-b)$ values exhibit velocity-strengthening behaviors and stable sliding. Otherwise, a negative $(a-b)$ value signifies a velocity-weakening behavior and an unstable sliding potential whenever the critical stiffness criterion is also met.

3. Results

3.1. Effect of obsidian content on gouge friction

The friction-displacement curves for the four gouges with varying mineral contents are presented in Fig. 2. Each test shows a similar linear increase in friction until approaching a state with a decrease in the rate of friction increase with slip at shear displacements of 1.0–1.5 mm, followed by a strain-hardening behavior, which is probably caused by increasing contact area resulting from particle crushing and shear compaction [4,32]. All friction-displacement curves have been detrended before deriving the RSF parameters to eliminate the effect of cumulative strain-hardening.

The coefficients of friction (μ) for the Group 1 tests are in the range of 0.70–0.74 (Fig. 3a, Table 2), consistent with prior studies (i.e., basalt μ–0.70 and obsidian μ–0.74) [15,22]. The frictional strengths of mixed or pure obsidian gouge show a negligible increase compared to pure basalt gouge. Frictional stability $(a-b)$ was recovered following the procedures described above and the results are shown in Table 2 and Fig. 3b. The values of $(a-b)$ monotonically decrease with increasing obsidian content, showing a transition from velocity-neutral on pure basalt gouge ($a-b$ = −0.0003 to 0.0011) to velocity-weakening on pure obsidian gouge ($a-b$ = −0.0041 to −0.0012).

3.2. Effect of temperature on gouge friction

Fig. 4 shows the friction-displacement curves for 20% obsidian +80% basalt mixed gouges at incremented temperatures, and the frictional strength is insensitive to temperature (~0.70–0.74) (Fig. 5a, Table 2), corresponding to the behavior of basalt gouges reported by Zhang et al. [22]. Notably, values of $(a-b)$ for mixed gouges fluctuate considerably with temperature, and the regularity is presented in Fig. 5b. $(a-b)$ values show a monotonic decrease (more negative) with increasing temperature to 250 °C. The mixed gouge exhibits an evident transition from velocity-strengthening at 100 °C ($a-b$ = −0.0001 to 0.0034) to velocity-neutral at 200 °C ($a-b$ = −0.0011 to 0.0006), to then velocity-weakening at 250 °C

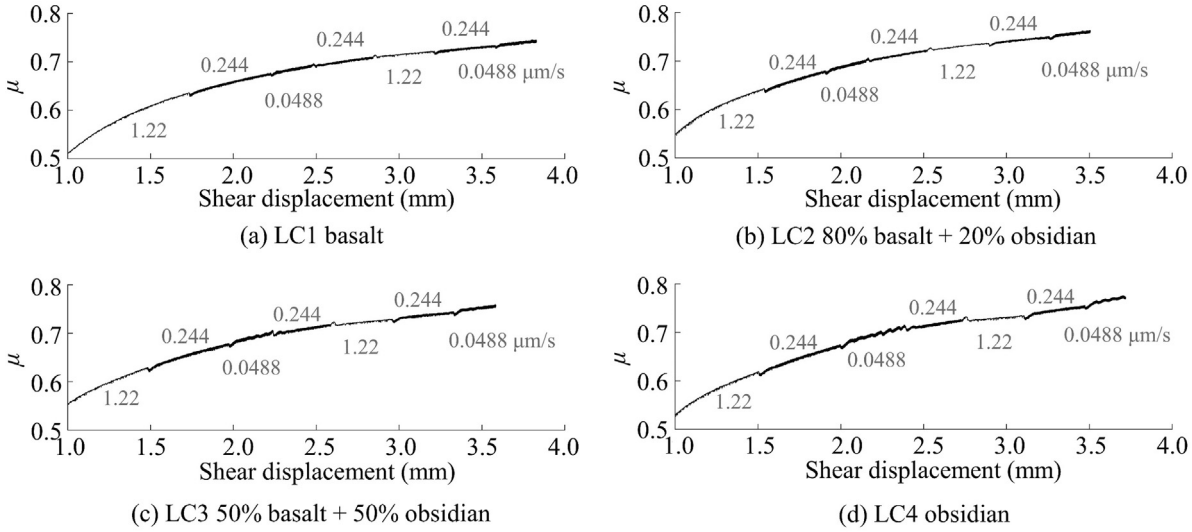

Fig. 2. Friction coefficient (μ) versus the shear displacement for basalt gouges with increasing obsidian content.

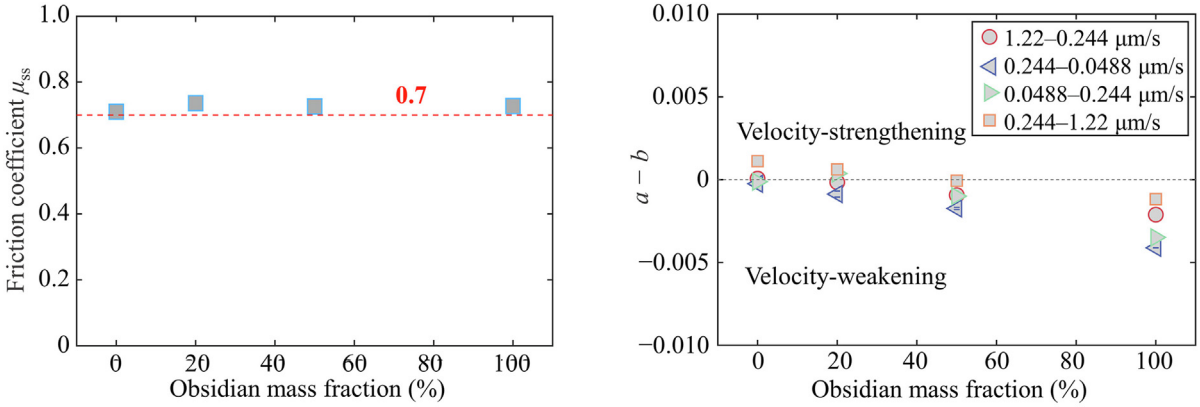

Fig. 3. Frictional parameters for basalt gouges with increasing obsidian content. Note: The friction coefficient was always estimated at the second applied shear velocity of 1.22 μm/s in each test. The error bars denote the standard deviations. The legend in (b) represents the shear rates.

Table 2
Results for friction coefficient (μ_{ss}) and frictional stability ($a - b$).

Test ID	μ_{ss}	$(a - b) \times 10^{-3}$ at axial displacement velocities (μm/s)			
		0.20–0.04	0.04–0.20	0.2–1.0	1.0–0.2
LC1	0.7100	−0.2±0.1	−0.1	1.1	0
LC2	0.7361	−0.9±0.2	0.4	0.6	−0.2
LC3	0.7262	−1.7±0.1	−1.0	−0.1	−0.9
LC4	0.7276	−4.1	−3.5	−1.2	−2.1
LC5	0.6994	0.2±0.2	2.3	3.4	1.4
LC6	0.7119	−1.9±0.2	0.4	0.6	−0.8
LC7	0.7294	−0.6±0.2	0.4	0.7	−0.4
LC8	0.7389	0.8±0.1	3.6	2.8	2.0
LC9	0.7293	−6.3±0.7	−3.6	−8.3	−8.8

Note: The friction coefficients (μ) were determined at a shear rate of 1.22 μm/s (~2.9 mm shear displacement). The frictional stability ($a-b$) values were averaged from the same velocity steps with the errors calculated based on the standard deviations in each test. The first velocity step (i.e., 1.220–0.244 μm/s) was removed from the calculation.

($a-b$ =−0.0021 to 0.0006) (Fig. 5b, Table 2). Conversely, ($a-b$) values increase with temperatures elevated above 250 °C, and the mixed gouge finally shows velocity-strengthening behavior at 400 °C ($a-b$ = 0.0007 to 0.0036), with a transition temperature of 300 °C showing velocity-neutral behavior ($a-b$ = −0.0008 to 0.0007) (Fig. 5b, Table 2). In previous studies, many gouges show similar temperature dependence of friction for granite [33,34], gabbro [19], plagioclase [21] and basalt gouges [22].

3.3. Effect of humidity on obsidian gouge friction

Fig. 6 shows the friction-displacement curves for the dry and wet obsidian gouge. The frictional strength of the pure obsidian gouge remains constant (~0.73) regardless of wet or dry conditions (Fig. 7a, Table 2). Notably, wet obsidian gouge shows apparent stick–slip at the lowermost shear velocities of 0.244 and 0.0488 μm/s and lower ($a-b$) values, indicating a potential of seismicity [35]. Our results on wet and dry obsidian gouges at the same effective confining stress emphasize the promotion of velocity weakening by water as a transfer medium and neglect the contribution of fluid pressure in impacting effective stress (Fig. 7b).

3.4. Microstructural characterization

Microstructural characterization (backscattered electron) was completed using scanning electron microscopy (SEM). Evolved microstructures of deformed gouges from Groups 1 and 2 are illustrated in Figs. 8 and 9 with standard nomenclature [36] adopted to describe the fabric of the deformed gouges.

The deformed microstructure for basalt/obsidian mixed gouges and pure basalt and obsidian gouges are shown in Fig. 8. Pure dry basalt and mixed gouges all exhibit pervasive R_1 (Riedel) fractures and moderate intensely sheared regions (ISRs) (Fig. 8), representative of moderate strain localization. The pure dry obsidian gouge is highly broken and exhibits numerous R_1 fractures and ISRs. The obsidian particles are strongly comminuted in these zones, indicating strong localized shear in response to velocity-weakening behavior (Fig. 8d).

For dry mixed gouges (80% basalt + 20% obsidian) at different temperatures (from 100 to 400 °C), the deformed gouges with velocity-neutral and velocity-weakening behaviors exhibit dense R_1 fractures and ISRs (Fig. 9). Mixed gouges at 100 and 400 °C show velocity-strengthening behaviors and correspondingly fewer R_1 fractures compared to mixed gouges at 200 to 300 °C, while homogeneous cataclastic flow is observed in the gouge at 400 °C.

4. Discussion

4.1. Effect of mineral composition on fault friction

Results for variable mineral compositions (Group 1 imply that homogeneous mixed dry basalt/obsidian gouges exhibit velocity-neutral behaviors when obsidian mass fractions are <50% (including pure basalt gouge and for our experimental conditions), while pure obsidian gouge exhibits velocity-weakening behavior (Fig. 3b). ($a-b$) values decrease monotonically with increasing obsidian content, contrary to the compositionally-independent friction coefficient (Fig. 3). This suggests that the presence of obsid-

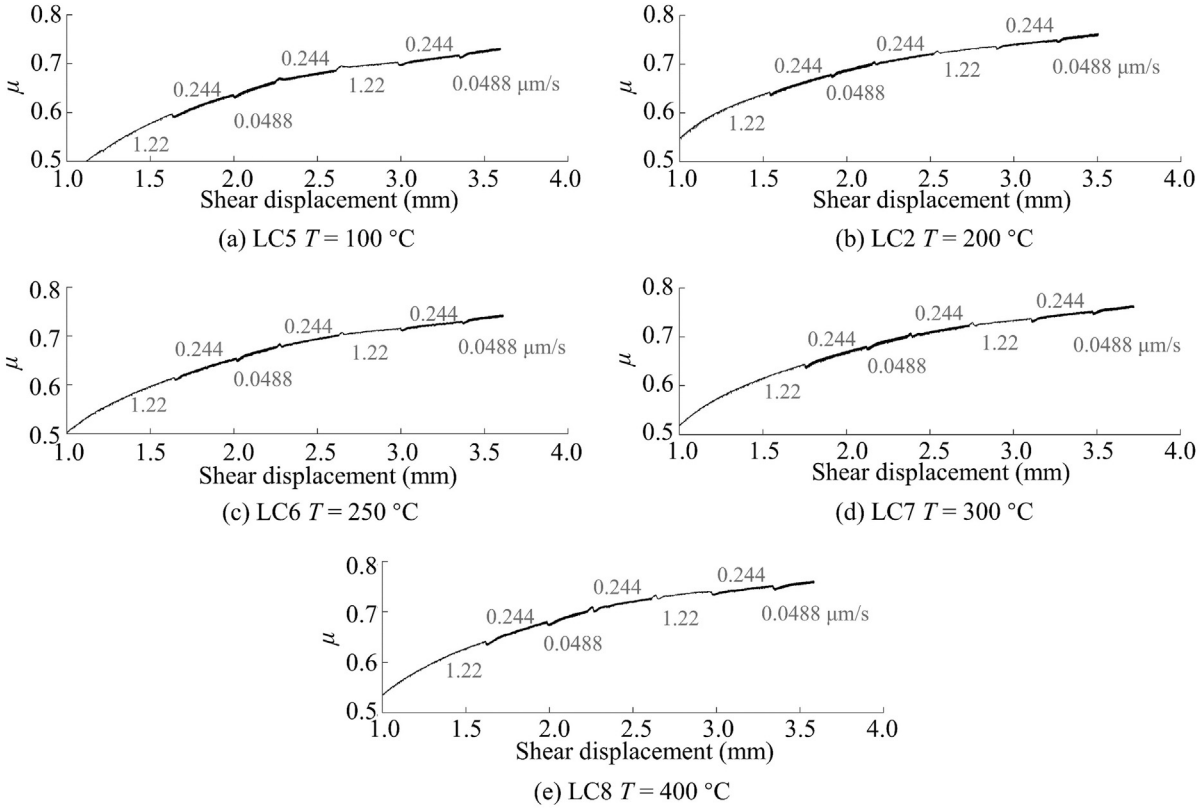

Fig 4. Friction coefficient (μ) versus the shear displacement for mixed gouges with varying temperatures.

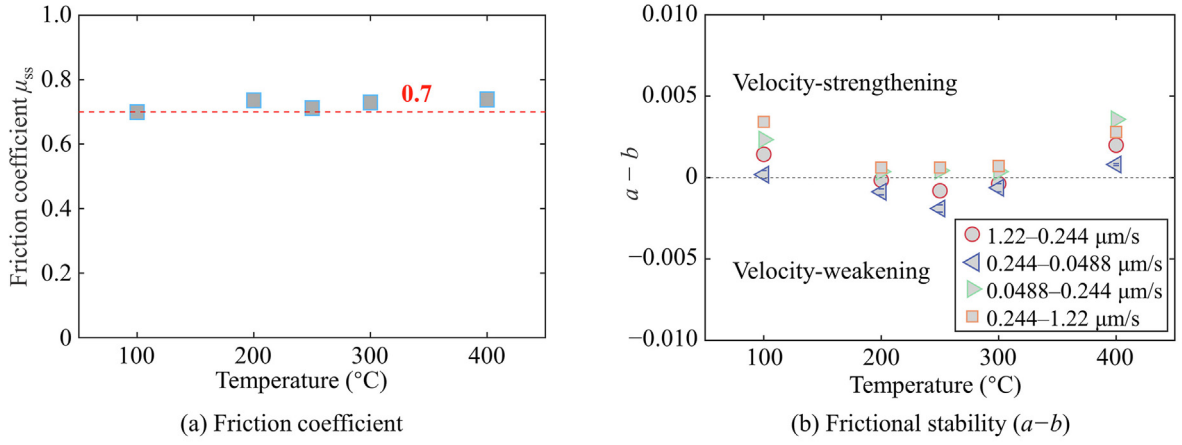

Fig. 5. Frictional parameters for mixed gouges at variable temperatures. Note: The friction coefficient was always estimated at the second applied shear rate of 1.22 μm/s in each test. The error bars denote the standard deviations. The legend in (b) represents the shear rates.

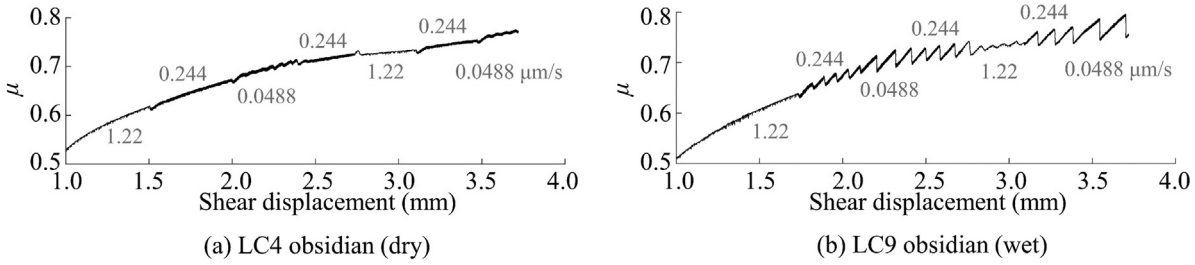

Fig. 6. Friction coefficient (μ) versus the shear displacement for Group 3 gouges.

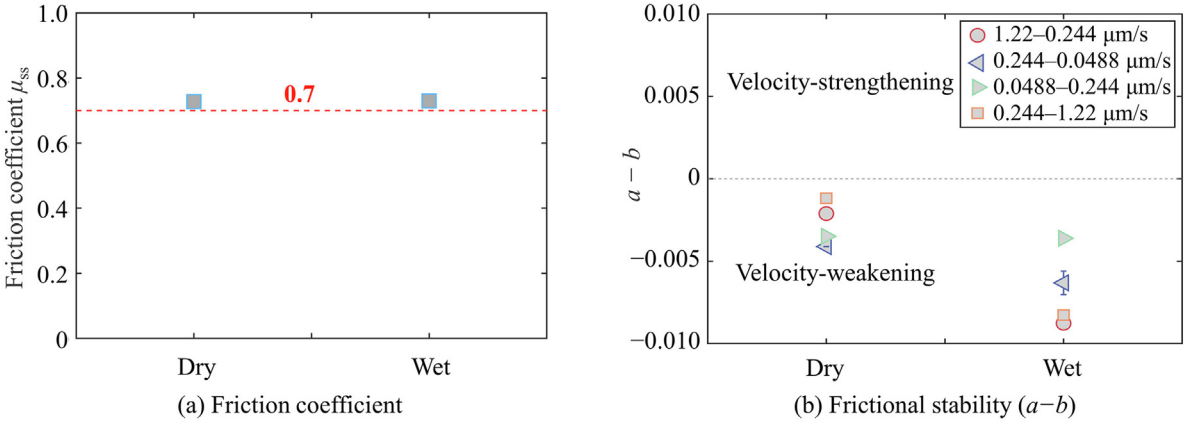

Fig. 7. Frictional parameters for Group 3 gouges. Note: The friction coefficient was always estimated at the second applied shear rate of 1.22 μm/s in each test. The error bars denote the standard deviations. The legend in (b) represents the shear rates.

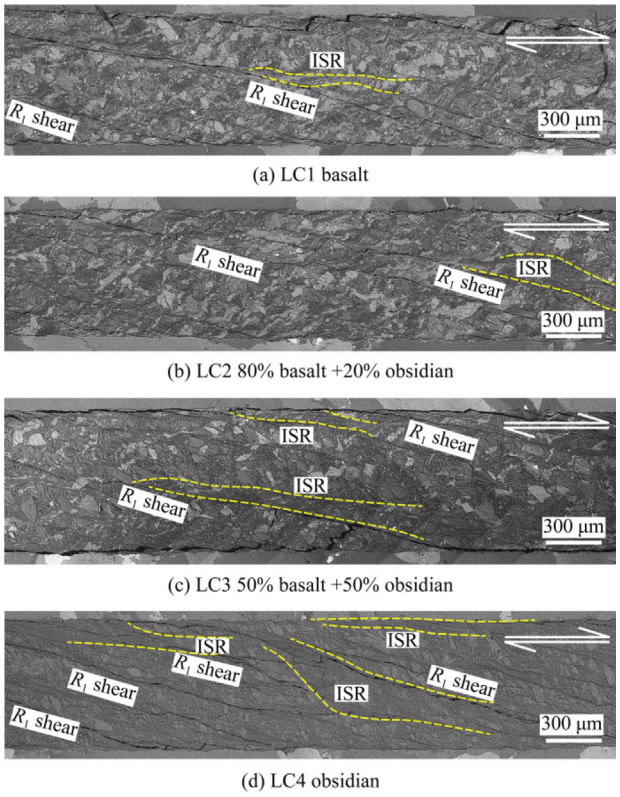

Fig. 8. Microstructures of the deformed basalt/obsidian mixed gouges. Note: Intensely sheared regions (ISRs) are delineated by the yellow dashed lines. (For interpretation of the references to colour in this figure legend, the reader is referred to the web version of this article.)

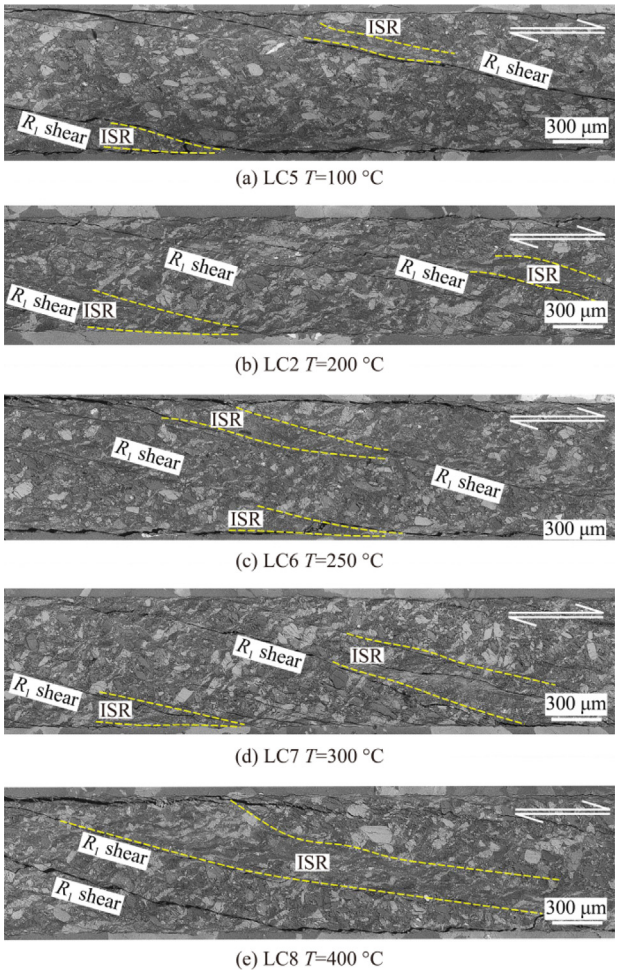

Fig. 9. Microstructures of the deformed 80% basalt + 20% obsidian gouges shearing at elevated temperatures. Note: Intensely sheared regions (ISRs) are delineated by the yellow dashed lines.

ian will not affect strength but may favor increased instability. Interstitial glass within basalt has been observed to promote unstable frictional behavior and rupture due to thermal softening [8] — although such results show that glassy minerals with a more significant crystal fraction elevate steady-state friction.

Fault materials with high percentages of brittle components (brittle-rich) tend to promote shear dilation [37], indicating higher porosity and then lower frictional strength at imposed high shear velocities — producing velocity-weakening behaviors [38]. Highly crushed obsidian particles characterized in the pure obsidian gouge also suggest this mechanism (Fig. 8d).

As noted by Violay et al. [8], possible weakening mechanisms of glassy rock are characterized by thermal softening above 500 °C and bulk melting above 1250 °C. However, these high temperatures are observed from high-velocity friction experiments at slip rates up to 6.5 m/s, which is substantially different from our low-velocity shear experiments at slip to only 1.22 μm/s and tem-

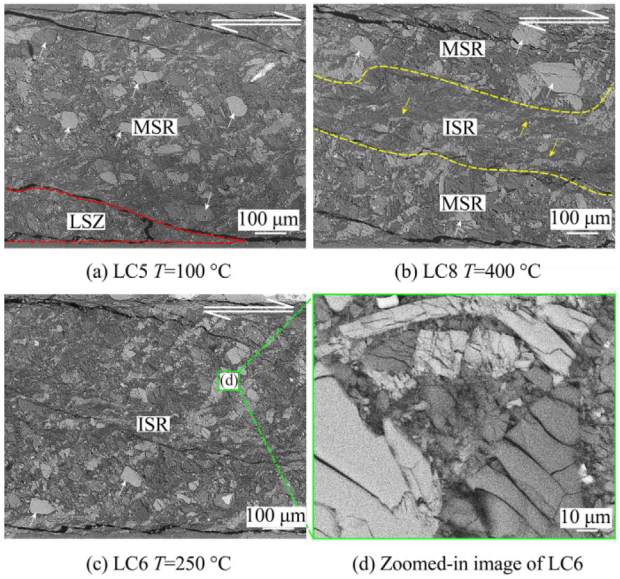

Fig. 10. Detailed microstructures of the deformed 80% basalt + 20% obsidian gouges shearing at different temperatures. Note: The localized shear zone (LSZ) is delineated by the red dashed lines. The large intensely sheared regions (ISR) and moderately sheared regions (MSR) are delineated by the yellow dashed lines. White arrows mark intact large-scale particles. Yellow arrows indicate intensely fractured hard clasts. (For interpretation of the references to colour in this figure legend, the reader is referred to the web version of this article.)

peratures up to 400 °C. Significantly, this observed mechanism [8] can be regarded as an informative extension that expands our results to a higher temperature range (at least temperatures >400 °C), where the involvement of glassy minerals may promote further weakening of the velocity-weakening faults at higher temperatures. Similarly, Proctor et al. [15] illustrated large stick–slip stress drops as the wet obsidian gouges translate from brittle to plastic at ~300 °C.

4.2. Impact of temperature on frictional stability

The shear experiments conducted at elevated temperatures (T=100 to 400 °C) reflect three regimes of shear behaviors as temperature is incremented — low-temperature velocity-strengthening behavior, transitioning to velocity-weakening behavior then reverting to velocity-strengthening behavior. Almost all typical mafic rock fault gouges exhibit velocity-strengthening behaviors at low temperatures (<150 °C) that then evolve to velocity-weakening behavior in the temperature range of 150–250 °C (e.g., [20–23]).

For the first transition from velocity-strengthening to velocity-weakening, the weakening behavior in our work may result from structural change — the formation of large R_1 shears with prominent surrounding zones of comminuted particles (Fig. 9c), which can result in strong shear localization and spatially heterogeneous slip rate within the shearing gouges [33], in response to shear dilation and localization-induced elevated porosity at high shear rates. Niemeijer and Spiers [27] also proposed the destruction of foliation in phyllosilicate-bearing gouges associated with velocity-weakening behaviors. Secondly, the mechanism of thermally activated compaction [39] will result in strong cataclasis of almost all large particles at high temperatures, similar to our observed microstructure for the deformed mixed gouge at 250 °C with the minimum (maximum negative) ($a-b$) value (Fig. 10c). The degree of large particle cataclasis in LC6 (250 °C) is significantly larger than that of LC5 (100 °C) and LC8 (400 °C), which retain many large and original intact particles (Fig. 10). Large-scale fragmented particles can be observed from the zoomed-in image of LC6 (Fig. 10d). This influence at increased temperature may result from the decrease in fracture resistance and increased propagation of subcritical cracks. These intensely crushed particles may contribute to an increased steady-state porosity (i.e., the dilation degree) and hence the lower frictional strength when increasing the shear rate – ultimately manifest as the observed velocity-weakening response.

The second transition from velocity-weakening to velocity-strengthening has been experimentally linked to increases in temperature [33,34], indicating a possible transition from elastic-brittle deformation to crystal plasticity in friction micromechanics [14,34]. Similarly, the brittle-plastic transition of the failure mode of basaltic faults was observed at elevated temperatures [22]. Indexed by friction constitutive parameters, dry mixed gouges at 100 and 400 °C signal velocity-strengthening behaviors with similar and negative ($a-b$) values. However, the different microstructures of these two deformed gouges suggest a potential change in deformation mechanism (Fig. 10). The microstructure of dry mixed gouge at 100 °C shows distributed particle crushing and a few R_1 fractures, each surrounded by a 10 to 40 μm thick intensely sheared zone. Large clasts with grain sizes in the range of 10–100 μm are embedded irregularly in the matrix of submicron-sized refined grains, demonstrating heterogeneous cataclastic deformation assisted by brittle rheology (Fig. 10a). Other dry shear experiments on quartz gouges at high temperatures [34] also exhibit homogeneous cataclastic flow with some minor R_1 shear, similar to our results for mixed gouges sheared at 400 °C (Fig. 10b). The homogeneous cataclastic flow zone (i.e., intensely sheared region), exhibits minor folds with extended "tails" along the shear direction and behind large crushed particles and is sandwiched between the heterogeneous cataclastic flow zones (i.e., moderately sheared regions), indicating a potential semibrittle state [40]. Conversely, Zhang et al. [22] noted that their dry plagioclase gouges with velocity-strengthening behavior at 617 °C only develop cataclastic granular flow instead of plastic flow. Thus, structural changes including significant shear localization and noticeable porosity decrease may be a vital control. Intensely fractured brittle particles are observed in our results which first experience fracture, then rotate and finally elongate along the shear direction (Fig. 10b). This type of thermally-enhanced cataclasis and the resulting strongly crushed grains may increase the capacity of highly distributed shear strain even more significantly than that of a localized shear zone. Similarly, plastic flow can accommodate increased shear strain and lead to velocity-strengthening behaviors. Hence, the attribution of velocity-strengthening behaviors at high temperatures in our study to these two mechanisms is reasonable and is consistent with prior studies.

Particularly, the addition of glassy minerals like obsidian within mafic rock gouges may change the transition temperatures for velocity-strengthening-to-velocity-weakening and then for velocity-weakening-to-velocity-strengthening by destabilizing the fault system. Additionally, fluid-assisted processes like IPS are inactive in dry faults, resulting in little dependence of frictional stability on shear velocity and temperature [23], that is, the absolute values of ($a-b$) derived from wet experiments are higher than those from dry experiments.

4.3. Implications for seismicity in basalt-bearing zones

Our results have significant implications in understanding seismicity in basalts, as present in lunar soil and crust, oceanic crust and on continents. Deep faults exist in ubiquitously high-temperature and high-pressure environments. Thus, the coupled effects of the temperature, stress and mineral composition are

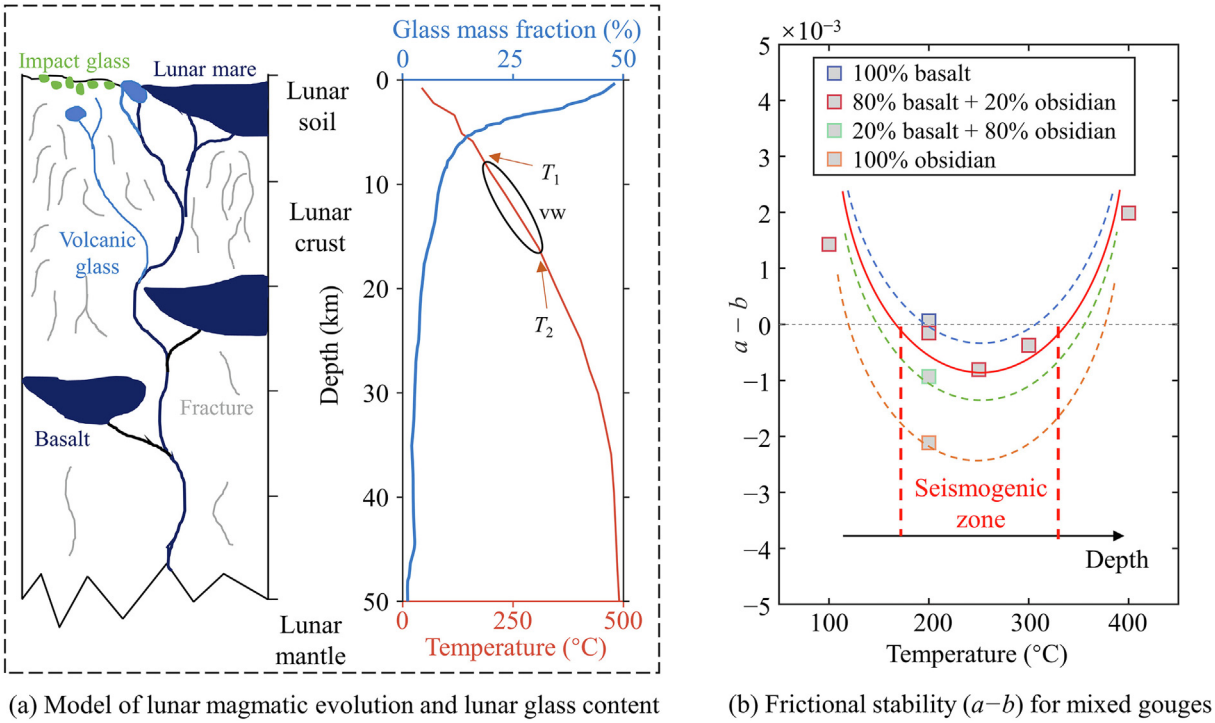

Fig. 11. Schematic model for lunar friction parameters versus temperature. Note: In (a), dark continuous lines represent feeder conduits for the melted lunar mantle (including molten mare basalt and volcanic glass). Green patches mark the impact glass and grey curve segments represent the fracture distribution within the lunar crust. The temperature profile of the lunar crust is a composite of prior speculative profiles. The curve of glass mass fractions is our inference, necessary due to the absence of observations of the exact glass content profile of the lunar crust. In (b), solid and dashed parabolas represent the trend of $(a-b)$ values versus temperature of 20% glassy basalt gouges and the predicted $(a-b)$ value trends of other basalt gouges with intermediate obsidian contents. The area surrounded by solid and dashed lines indicates the anticipated depth range of the seismogenic zone. (For interpretation of the references to colour in this figure legend, the reader is referred to the web version of this article.)

important in defining the frictional properties, especially the frictional strength and stability — towards understanding the potential for seismicity. It is worth noting that inferences from our observed frictional properties of basaltic and glassy minerals may not be applicable to ductile mylonitic shear zones.

Based on the temperature-depth curves of the moon and the identification of different types of glasses from Apollo lunar soil [11], we systematically explore potential habits of seismicity in the full-depth lunar crust (Fig. 11a). Impact moonquakes caused by asteroid impact only occur within that lunar regolith and will be shallow [41] — we do not consider these. Rutherford et al. [42] have established a model for lunar magma ascent dynamics and indicated that the melt glasses were quenched at pressures from 17 to 2 MPa representing depths of 4 to 0.5 km in the lunar crust, indicating that volcanic glass (i.e., obsidian) in the lunar crust is almost all distributed shallower than ~5 km depth. At shallow depths (<10 km), high glass-content-related velocity-weakening behaviors and low-temperature-related velocity-strengthening behaviors lead to an ambiguous definition of fault stability. However, the structurally disturbed crust containing relatively intricate fracture networks provides the opportunity to host seismicity [43]. As the depth increases to ~15 km, the temperature exceeds the transition T_1 from velocity-strengthening to velocity-weakening and the glasses (generally consisting of pure volcanic glass) are in significantly lower proportion to that of lunar soil and the shallower lunar crust (Fig. 11a). It remains undefined whether the temperature- or the mineralogic-effect dominates in controlling fault stability, due to the imprecise/unknown abundances and distributions of glass at this depth regime. Deeper, and within the lower part of the lunar crust, temperature increases significantly while glass content decreases, but seismic events appear less likely owing to sparsely distributed faults (at higher confining stresses) and the reported transition from brittle-to-ductile behavior of basalt at high temperatures [22]. Our results infer that shallow moonquakes should dominate the observational record with deeper lunar crust less likely to be seismic. Similarly, Watters et al. [44] demonstrated that the Moon is tectonically active and that the shallow moonquakes are strongly related to the activity of young thrust faults which are present from the surface down to depths of hundreds of meters [45]. However, Gillet et al. [46] noted that shallow moonquakes originate from depths of (50±20) km within the lunar crust (i.e., the deeper lunar crust and result from slip on deep faults).

However, the three temperature/depth regimes corresponding to the different frictional stabilities likely dominate control of the distribution of seismic events. The transition temperature T_2 (from velocity-weakening behavior to velocity-strengthening behavior) of granite gouge is reported to be 350 °C [33], driving a reasonable explanation for the cut-off depth of minor seismic events on the San Andreas Fault. Granite gouges from the Gonghe geothermal reservoir exhibit a similar temperature range of 150 to 250 °C corresponding to velocity-weakening behaviors [47]. The transition temperature T_2 of the Nankai subduction zone is estimated at 350 °C as the maximum temperature for seismic initiation [48]. The T_2 of dry glass-bearing basaltic gouges found in our study is 300 °C, relevant to temperatures expected at ~10 km in the terrestrial crust, which can be considered a typical cut-off depth of small earthquakes nucleated in glass-bearing basaltic faults. Our results for mixed gouges with elevated obsidian contents identify a lower T_1 and a higher T_2, indicating a wider temperature range, that is, a larger depth range of velocity-weakening behaviors (i.e., a seismogenic zone with potentially seismic events) (Fig. 11b). In addition, the presence of water has a negligible effect on the transition temperature [33]. However, the weakening effect of water, including

both the effects of pressure solution and the decreased effective stress (and therefore frictional strength), must be evaluated to better understand earthquake nucleation and avoid seismic hazards.

5. Conclusions

We systematically measured the frictional strength and stability of glass-bearing dry basaltic gouges with elevated obsidian content and mixed basalt/obsidian gouges at incremented temperatures spanning 100 to 400 °C together with pure obsidian gouge under hydrothermal conditions. These experiments were used to separately investigate the impacts of mineral composition, temperature and humidity on frictional and stability response. We derive the following conclusions from these laboratory observations:

(1) The frictional strengths of glass-bearing basalt gouges with increasing obsidian contents — from pure basalt gouge to pure obsidian gouge — are high (0.70–0.74) with no clear trend with mineral content. The observed transition from velocity-neutral behavior of pure basalt gouge to velocity-weakening behavior of pure obsidian gouge suggests an impact of weakening by glassy minerals and its impact on frictional stability. This impact can be attributed to low frictional strength due to high porosity, driven by dilation and caused by highly fractured obsidian particles at high slip rates.
(2) The mixed 80% basalt + 20% obsidian gouges exhibit two composite trends over the span of temperatures 100 to 400 °C: (i) From velocity-strengthening at 100 °C to velocity-neutral at 200 °C, then velocity-weakening to a minimum ($a-b$) at 250 °C; then, (ii) From this maximum velocity-weakening at 250 °C to velocity-neutral at 300 °C and finally velocity-strengthening at 400 °C. The first transition can be interpreted as shear localization or thermally activated compaction and the second transition may be due to the coupled effect of plastic flow and microstructural changes at high temperatures.
(3) The weakening effect of water as a mass transfer agent or high-pressure pore fluid as a strength reduction agent is an essential control governing frictional stability in deformed gouges under hydrothermal conditions.
(4) The transition temperature of basaltic faults from velocity-weakening to velocity-strengthening behavior determines the cut-off depth for seismic events and thus the presence of glass may increase this span in depths for the seismogenic zone.

Acknowledgements

This research was funded by the National Natural Science Foundation of China (Nos. 42320104003 and 42107163), the Fundamental Research Funds for the Central Universities. Derek Elsworth acknowledges support from the G. Albert Shoemaker endowment. We appreciate the assistance of Changrong He, Wenming Yao, and Shimin Liu in lab.

Supplementary data

The shear displacement and coefficient of friction data for LC1–LC9 can be found at: https://doi.org/10.1016/j.ijmst.2024.04.012.

References

[1] Anderson Jr AT. Parental basalts in subduction zones: implications for continental evolution. J Geophys Res 1982;87(B8):7047–60.
[2] Walker D. Lunar and terrestrial crust formation. J Geophys Res 1983;88(S01):17–25.
[3] Saito T, Ewing M, Burckle LH. Tertiary sediment from the mid-Atlantic ridge. Science 1966;151(3714):1075–9.
[4] Scholz CH. Mechanics of faulting. The mechanics of earthquakes and faulting. Cambridge: Cambridge University Press; 2002. p. 101–78.
[5] Nunn C, Garcia RF, Nakamura Y, Marusiak AG, Kawamura T, Sun DY, et al. Lunar seismology: A data and instrumentation review. Space Sci Rev 2020;216(5):89.
[6] Nakamura Y. Shallow moonquakes: how they compare with earthquakes. In: Lunar and Planetary Science Conference, 11th. Houston: Lunar and Planetary Science Conference; 1980. p. 1847–53.
[7] Rudnick RL, Fountain DM. Nature and composition of the continental crust: A lower crustal perspective. Rev Geophys 1995;33(3):267–310.
[8] Violay M, Di Toro G, Gibert B, Nielsen S, Spagnuolo E, Del Gaudio P, et al. Effect of glass on the frictional behavior of basalts at seismic slip rates. Geophys Res Lett 2014;41(2):348–55.
[9] Taylor LA, Pieters C, Patchen A, Taylor DHS, Morris RV, Keller LP, et al. Mineralogical and chemical characterization of lunar highland soils: insights into the space weathering of soils on airless bodies. J Geophys Res Planets 2010;115(2):1–14.
[10] Li CL, Hu H, Yang MF, Pei ZY, Zhou Q, Ren X, Liu B, Liu DW, Zeng XG, Zhang GG, Zhang HB, Liu JJ, Wang Q, Deng XJ, Xiao CJ, Yao YG, Xue DS, Zou W, Su Y, Wen WB, Ouyang ZY. Characteristics of the lunar samples returned by the Chang'e-5 mission. Natl Sci Rev 2021;9(2):nwab188.
[11] Delano JW. Pristine lunar glasses: Criteria, data, and implications. J Geophys Res 1986;91(B4):201–13.
[12] Kameda J, Inoue S, Tanikawa W, Yamaguchi A, Hamada Y, Hashimoto Y, Kimura G. Alteration and dehydration of subducting oceanic crust within subduction zones: implications for décollement step-down and plate-boundary seismogenesis. Earth Planets Space 2017;69(1):52.
[13] Di Toro G, Hirose T, Nielsen S, Pennacchioni G, Shimamoto T. Natural and experimental evidence of melt lubrication of faults during earthquakes. Science 2006;311(5761):647–9.
[14] Dieterich JH, Kilgore BD. Direct observation of frictional contacts: New insights for state-dependent properties. Pure Appl Geophys 1994;143(1):283–302.
[15] Proctor BP, Lockner DA, Lowenstern JB, Beeler NM. Conversion of wet glass to melt at lower seismogenic zone conditions: Implications for pseudotachylyte creep. Geophys Res Lett 2017;44(20):10248–55.
[16] Weeks JD, Beeler NM, Tullis TE. Frictional behavior: Glass is like a rock. Eos Trans AGU 1991;72:457–8.
[17] Webb S. Silicate melts: Relaxation, rheology, and the glass transition. Rev Geophys 1997;35(2):191–218.
[18] Kohlstedt DL, Evans B, Mackwell SJ. Strength of the lithosphere: constraints imposed by laboratory experiments. J Geophys Res 1995;100(B9):17587–602.
[19] He CR, Yao WM, Wang ZL, Zhou YS. Strength and stability of frictional sliding of gabbro gouge at elevated temperatures. Tectonophysics 2006;427(1–4):217–29.
[20] He CR, Luo L, Hao QM, Zhou YS. Velocity-weakening behavior of plagioclase and pyroxene gouges and stabilizing effect of small amounts of quartz under hydrothermal conditions. J Geophys Res Solid Earth 2013;118(7):3408–30.
[21] He CR, Tan WB, Zhang L. Comparing dry and wet friction of plagioclase: Implication to the mechanism of frictional evolution effect at hydrothermal conditions. J Geophys Res Solid Earth 2016;121(9):6365–83.
[22] Zhang L, He CR, Liu YJ, Lin J. Frictional properties of the South China Sea oceanic basalt and implications for strength of the Manila subduction seismogenic zone. Mar Geol 2017;394:16–29.
[23] Okuda H, Niemeijer AR, Takahashi M, Yamaguchi A, Spiers CJ. Hydrothermal friction experiments on simulated basaltic fault gouge and implications for megathrust earthquakes. JGR Solid Earth 2023;128(1):1–23.
[24] Karato SI. Geophysical constraints on the water content of the lunar mantle and its implications for the origin of the Moon. Earth Planet Sci Lett 2013;384:144–53.
[25] Revil A. Pervasive pressure solution transfer in a quartz sand. J Geophys Res 2001;106(B5):8665–86.
[26] Yasuhara H, Elsworth D, Polak A. A mechanistic model for compaction of granular aggregates moderated by pressure solution. J Geophys Res Solid Earth 2003;108(B11):2530.
[27] Niemeijer AR, Spiers CJ. A microphysical model for strong velocity weakening in phyllosilicate-bearing fault gouges. J Geophys Res 2007;112(B10):1–12.
[28] Li RL, Zhou GQ, Yan K, Chen J, Chen DQ, Cai SY, et al. Preparation and characterization of a specialized lunar regolith simulant for use in lunar low gravity simulation. Int J Min Sci Technol 2022;32(1):1–15.
[29] Hao HC, Gao MZ, Li CB, Wang X, Wu Y, Gao Z, et al. Selection and thermal physical characteristics analysis of *in situ* condition preserved coring lunar rock simulant in extreme environment. Int J Min Sci Technol 2023;33(11):1411–24.
[30] Dieterich J. Modeling of rock friction: Experimental results and constitutive equations. J Geophys Res 1979;84:2161–8.
[31] Ruina A. Slip instability and state variable friction laws. J Geophys Res 1983;88(B12):10359–70.

[32] Tembe S, Lockner DA, Wong TF. Effect of clay content and mineralogy on frictional sliding behavior of simulated gouges: Binary and ternary mixtures of quartz, illite, and montmorillonite. J Geophys Res 2010;115(B3):1–22.
[33] Blanpied ML, Lockner DA, Byerlee JD. Frictional slip of granite at hydrothermal conditions. J Geophys Res 1995;100(B7):13045–64.
[34] Chester FM, Higgs NG. Multimechanism friction constitutive model for ultrafine quartz gouge at hypocentral conditions. J Geophys Res 1992;97(B2):1859–70.
[35] Brace WF, Byerlee JD. Stick-slip as a mechanism for earthquakes. Science 1966;153(3739):990–2.
[36] Logan JM, Dengo CA, Higgs NG, Wang ZZ. Chapter 2 fabrics of experimental fault zones: their development and relationship to mechanical behavior. In: International Geophysics. Amsterdam: Elsevier; 1992. p. 33–67.
[37] Marone C, Kilgore B. Scaling of the critical slip distance for seismic faulting with shear strain in fault zones. Nature 1993;362(6421):618–21.
[38] Samuelson J, Elsworth D, Marone C. Shear-induced dilatancy of fluid-saturated faults: experiment and theory. J Geophys Res Solid Earth 2009;114(B12):B12404.
[39] Zhang L, He CR. Frictional properties of phyllosilicate-rich mylonite and conditions for the brittle-ductile transition. J Geophys Res Solid Earth 2016;121(4):3017–47.
[40] Jia CJ, Zhang S, Xu WY. Experimental investigation and numerical modeling of coupled elastoplastic damage and permeability of saturated hard rock. Rock Mech Rock Eng 2021;54(3):1151–69.
[41] Kumar PS, Mohanty R, Lakshmi KJP, Raghukanth STG, Dabhu AC, Rajasekhar RP, et al. The seismically active lobate scarps and coseismic lunar boulder avalanches triggered by 3 January 1975 (M_W 4.1) shallow moonquake. Geophys Res Lett 2019;46(14):7972–81.
[42] Rutherford MJ, Head JW, Saal AE, Hauri E, Wilson L. Model for the origin, ascent, and eruption of lunar picritic magmas. Am Mineral 2017;102(10):2045–53.
[43] Watters TR, Robinson MS, Beyer RA, Banks ME, Bell JF, Pritchard ME, Hiesinger H, van der Bogert CH, Thomas PC, Turtle EP, Williams NR. Evidence of recent thrust faulting on the Moon revealed by the Lunar Reconnaissance Orbiter Camera. Science 2010;329(5994):936–40.
[44] Watters TR, Weber RC, Collins GC, Howley IJ, Schmerr NC, Johnson CL. Shallow seismic activity and young thrust faults on the Moon. Nat Geosci 2019;12:411–7.
[45] Williams NR, Watters TR, Pritchard ME, Banks ME, Bell III JF. Fault dislocation modeled structure of lobate scarps from Lunar Reconnaissance Orbiter Camera digital terrain models. JGR Planets 2013;118(2):224–33.
[46] Gillet K, Margerin L, Calvet M, Monnereau M. Scattering attenuation profile of the Moon: Implications for shallow moonquakes and the structure of the megaregolith. Phys Earth Planet In 2017;262:28–40.
[47] Zhang FS, Cao ST, An MK, Zhang CY, Elsworth D. Friction and stability of granite faults in the Gonghe geothermal reservoir and implications for injection-induced seismicity. Geothermics 2023;112:102730.
[48] Hyndman RD, Wang K, Yamano M. Thermal constraints on the seismogenic portion of the southwestern Japan subduction thrust. J Geophys Res 1995;100(B8):15373–92.